AFRL-RX-WP-TP-2011-4209

MICROSTRUCTURE AND TEXTURE EVOLUTION DURING HOT PACK ROLLING OF NICKEL-BASE SUPERALLOYS TO THIN SHEET AND FOIL (PREPRINT)

D.L. Ballard, D.S. Weaver, and S.L. Semiatin

Metals Branch
Metals, Ceramics, and NDE Division

A.L. Pi1chak

Universal Technology Corporation

MARCH 2011

AIR FORCE RESEARCH LABORATORY
MATERIALS AND MANUFACTURING DIRECTORATE
WRIGHT-PATTERSON AIR FORCE BASE, OH 45433-7750
AIR FORCE MATERIEL COMMAND
UNITED STATES AIR FORCE

REPORT DOCUMENTATION PAGE

Form Approved
OMB No. 0704-0188

1. REPORT DATE *(DD-MM-YY)*	2. REPORT TYPE	3. DATES COVERED *(From - To)*
March 2011	Journal Article Preprint	01 March 2011 – 01 March 2011

4. TITLE AND SUBTITLE

MICROSTRUCTURE AND TEXTURE EVOLUTION DURING HOT PACK ROLLING OF NICKEL-BASE SUPERALLOYS TO THIN SHEET AND FOIL (PREPRINT)

5a. CONTRACT NUMBER
In-house

5b. GRANT NUMBER

5c. PROGRAM ELEMENT NUMBER
62102F

6. AUTHOR(S)

D.L. Ballard, D.S. Weaver, and S.L. Semiatin (AFRL/RXLM)
A.L. Pilchak (Universal Technology Corporation)

5d. PROJECT NUMBER
4347

5e. TASK NUMBER
02

5f. WORK UNIT NUMBER
25100102

7. PERFORMING ORGANIZATION NAME(S) AND ADDRESS(ES)

Metals Branch (AFRL/RXLM)
Metals, Ceramics, and NDE Division
Air Force Research Laboratory
Materials and Manufacturing Directorate
Wright-Patterson Air Force Base, OH 45433-7750
Air Force Materiel Command
United States Air Force

Universal Technology Corporation
Dayton, OH 45432

8. PERFORMING ORGANIZATION REPORT NUMBER
AFRL-RX-WP-TP-2011-4209

9. SPONSORING/MONITORING AGENCY NAME(S) AND ADDRESS(ES)

Air Force Research Laboratory
Materials and Manufacturing Directorate
Wright-Patterson Air Force Base, OH 45433-7750
Air Force Materiel Command
United States Air Force

10. SPONSORING/MONITORING AGENCY ACRONYM(S)
AFRL/RXLM

11. SPONSORING/MONITORING AGENCY REPORT NUMBER(S)
AFRL-RX-WP-TP-2011-4209

12. DISTRIBUTION/AVAILABILITY STATEMENT
Approved for public release; distribution unlimited.

13. SUPPLEMENTARY NOTES

PAO Case Number: 88ABW 2010-2696; Clearance Date: 19 May 2010.
Journal article submitted to *Metallurgical and Materials Transactions A.*

14. ABSTRACT

Microstructure evolution during hot pack rolling of nickel-base superalloys to -l-mm thick sheet and -200-µm-thick foil was investigated with electron backscatter diffraction. The microstructure was observed at increasing levels of strain which revealed the progressive formation of an unrecrystallized, banded microstructure at sheet gage. The bands contained large orientation gradients, sometimes spanning multiple texture components that are considered to be stable with respect to the imposed plane-strain compression. Upon reaching stable orientations, grain-scale shear bands were observed within individual unrecrystallized bands that resulted in local subgrain rotations that formed new bands of different orientation. This phenomenon, known as band splitting in the literature, was shown to be the result of continuous dynamic recrystallization as opposed to discontinuous dynamic recrystallization or classical static recrystallization. The unrecrystallized bands were eliminated by unidirectional rolling to foil, but not by cross rolling.

15. SUBJECT TERMS
microstructure, hot pack rolling, nickel-base superalloys, thin sheet, foil

16. SECURITY CLASSIFICATION OF:			17. LIMITATION OF ABSTRACT:	18. NUMBER OF PAGES	19a. NAME OF RESPONSIBLE PERSON (Monitor)
a. REPORT	b. ABSTRACT	c. THIS PAGE			Donna L. Ballard
Unclassified	Unclassified	Unclassified	SAR	38	19b. TELEPHONE NUMBER *(Include Area Code)* N/A

Microstructure and Texture Evolution during Hot Pack Rolling of Nickel-Base Superalloys to Thin Sheet and Foil

A.L. Pilchak[1,2], D.L. Ballard[1], D.S. Weaver[1], and S.L. Semiatin[1]

[1]Air Force Research Laboratory, Materials and Manufacturing Directorate,
AFRL, RXLM, Wright Patterson Air Force Base, OH 45433

[2]Universal Technology Corporation, Dayton OH 45432

Abstract

Microstructure evolution during hot pack rolling of nickel-base superalloys to ~1-mm thick sheet and ~200-μm thick foil was investigated with electron backscatter diffraction. The microstructure was observed at increasing levels of strain which revealed the progressive formation of an unrecrystallized, banded microstructure at sheet gage. The bands contained large orientation gradients, sometimes spanning multiple texture components that are considered to be stable with respect to the imposed plane-strain compression. Upon reaching stable orientations, grain-scale shear bands were observed within individual unrecrystallized bands that resulted in local subgrain rotations that formed new bands of different orientation. This phenomenon, known as band splitting in the literature, was shown to be the result of continuous dynamic recrystallization as opposed to discontinuous dynamic recrystallization or classical static recrystallization. The unrecrystallized bands were eliminated by unidirectional rolling to foil, but not by cross rolling.

To updated before submission to journal: 5C gamma prime solvus temperature (Pg. 5 and Table I) based on more controlled heat treatments.

I. Introduction

Deformation and recrystallization textures of face-centered-cubic (FCC) metals subjected to plane-strain compression (PSC) have been the subject of much research [Zhou 1992; Maurice 1993; Driver 1994; Maurice 1997a; Maurice 1997b; Necker 1997; Samajdar 1998; Caleyo 2001; Sokolov 2005]. This research has focused on a wide range of alloy compositions (aluminum, copper, and nickel), deformation temperatures (cold, warm, and hot rolling), and total reductions. The resultant textures all share a common feature. In particular, analysis of the orientation distribution has revealed the presence of a cube texture following deformation which tends to increase in intensity with further straining and during subsequent recrystallization heat treatment. Often, the cube component, which aligns a {100} plane with the rolling plane and a <001> direction with the rolling direction, is referred to as a recrystallization-texture component although it is usually present at low intensities in the deformation texture as well [Hirsch 1988]. The intensity of the cube component in the deformation texture or recrystallization texture depends strongly on alloy composition and rolling temperature [Sokolov 2005].

The mechanism controlling the formation of the cube texture has been the subject of a long debate [Humphrey's book; Samajdar 1998]. One hypothesis, referred to as oriented nucleation (ON), postulates a frequency advantage of cube-oriented nuclei over those in other orientations; i.e., cube-oriented nuclei predominate in the deformed structure prior to recrystallization heat treatment. The frequency advantage is quantified by the factor $\alpha = \alpha_o/\alpha_r$, in which α_o denotes the fraction of cube-oriented grains in the recrystallized microstructure, and α_r is the cube fraction in a randomly-textured material. In an alternate interpretation, known as preferential or oriented growth, cube-oriented grains grow more quickly than those in other orientations and thus constitute a greater total volume fraction of the recrystallized microstructure. The size advantage is described by the factor β^3; β is defined as the ratio of the cube to non-cube grain sizes (diameters). As discussed by Samajdar and Doherty [Samajdar 1998], these factors can be used to quantify the relative importance of each mechanism regardless of their physical origin, thus making them unbiased parameters.

While PSC deformation and recrystallization textures of FCC metals have been frequently investigated, the *spatial distribution* of the grains constituting the various texture components has been reported less often. A notable exception is contained in the work of Samajdar and Doherty [Samajdar 1998], who described the formation of a banded microstructure during PSC and plane-strain extrusion of commercial-purity aluminum. The bands were quantified by acquiring line profiles in the sheet normal direction (orthogonal to

the bands) with electron backscatter diffraction (EBSD). The grains within the bands were in orientations consistent with typical PSC deformation-texture components. However, many cube- (or near-cube-) oriented bands were found to be relatively stable, especially at larger strains, despite being predicted as unstable by crystal-plasticity simulations [Samajdar 1998]. Transmission electron microscopy (TEM) analysis of the substructure revealed that bands in the S orientation {123}<634> had consistently higher average subgrain misorientation (~6°) than those in bands of other orientations. Smaller misorientations (i.e., between 1° and 2°) were measured within the cube-oriented bands, indicating that they had lower stored energy which gave rise to a strong frequency advantage of cube nuclei. Accordingly, this was the mechanism identified as leading to the intense cube recrystallization texture after heat treatment. Using a conservation of volume argument, Samajdar and Doherty also showed that one cube-oriented grain gave rise to at least one cube-oriented band, while those in other orientations split into seven strongly-misoriented bands after 50 pct. reduction. Upon further reduction, the number of bands remained approximately constant, but they were progressively thinned with increasing strain. The physical mechanism for band splitting was not addressed in detail, however.

Utilizing channel-die compression of pure aluminum and Al-1Mn single crystals and polycrystals, Maurice and Driver [Maurice 1993; Maurice 1997a] also observed band splitting. These authors found that (001)<110>-oriented crystals systematically decomposed into two complementary {112}<111> oriented bands by {111}<110> octahedral slip over a range of strain rates and deformation temperatures. In contrast, cube-oriented bands were stabilized during hot rolling ($T > 0.6T_m$) of aluminum alloys to strains as large as 1.5 due to non-octahedral slip on two {110}<110> systems. At temperatures below which the cube orientation was stabilized, "transition bands" were observed which had intermediate orientations between the parent and split band, signifying that the bands were the result of slip-induced lattice rotations.

Sokolov, *et al.* [Sokolov 2005] have described the formation of a similar banded structure during rolling of commercial-purity nickel and a variety of binary nickel-X alloys (where X = Cr, Mo, V, W) at temperatures of 20 and 200°C. The banded regions consisted of grains of nominally the same orientation that were elongated in the rolling direction. Using EBSD, each of the bands was linked to one of the stable FCC PSC deformation-texture components, although no cube-oriented bands were observed. TEM analysis of the banded regions revealed that they consisted of a "cellular dislocation structure" with a cell size of approximately 1 to 1.5 μm. The specific misorientation between adjacent cells was not reported. The authors also described the formation of shear bands within individual bands of similar orientation, but

unfortunately, these could not be quantified by the EBSD analysis. (Here, the term shear band is used to imply "microscopic shear bands" which traverse only one or a few grains in accordance with the terminology used by Canova, *et al.* [Canova 1984]). With regard to texture, Sokolov, *et al.* [Sokolov 2005] noted an increased volume fraction of cube orientations in the deformation texture for rolling at 200°C compared to the room-temperature results, although it was not clear if the cube-oriented grains were arranged in bands. Sokolov, *et al.* also noted that an increase in rolling temperature or the concentration of alloying elements reduced the intensity of the {110}<112> component in favor of {112}<111>. This resulted in a decrease in the intensity of the cube component upon recrystallization heat treatment, apparently due to a reduction in an oriented nucleation within the {110}<111> bands. In other work, Qu, *et al.* [Qu 2006] showed that hot rolling of 99.9 pct. pure nickel to a 35-pct. reduction followed by cold rolling to 99 pct. reduction produced a strong brass texture which formed an even stronger cube texture upon recrystallization.

While there have been numerous observations of banded microstructures in pure and moderately-alloyed aluminum and nickel, there are very limited data for the hot rolling of commercial nickel-base superalloys. One exception is the work of Park, *et al.* [Park 1997], who reported the effect of hot-rolling practice on the mechanical properties and recrystallization behavior of MA 754 (Special Metals Corp.). They observed high-aspect-ratio, submicron grains that were elongated in the rolling direction, but did not determine their orientations. In a related effort, Lee, *et al.* [Lee 1999] investigated the texture of the material hot rolled by Park, *et al.* [Park 1997]. Optical micrographs indicated a microstructure with bands that were one to several millimeters long. Hot rolling textures were measured with x-ray diffraction from which orientation distributions were calculated and analyzed. The results revealed that the Goss orientation {110}<001> was dominant in the as-rolled microstructure at all levels of reduction. No significant cube orientation was present in the as-rolled condition or after recrystallization.

Recently, Ballard et al. [Ballard JECS] demonstrated successful hot pack rolling of a γ'-strengthened, platinum-group-metal (PGM) modified nickel-base superalloy to 1 mm thick sheet and 250 μm foil. Unrecrystallized bands were observed in the rolled sheet. It was speculated that the bands may have been formed by flattening and elongation of coarse, unrecrystallized grains present in the starting forged structure. However, in the present research, it was determined that the fraction of unrecrystallized grains in the forged condition was too small to account for the number of bands in the rolled sheet. Thus, EBSD was used to clarify the mechanism by which the banded microstructure is formed from an equiaxed starting

microstructure, how the bands evolve, and how they eventually split into highly-misoriented bands over a large range of strain. The program materials investigated here were a PGM-modified nickel-base superalloy and an alloy with the same composition but without the addition of PGM elements. PGM-modified alloys are currently being evaluated as oxidation-resistant materials for thermal protection systems [Ballard JECS]. Coupland, *et al.* [Coupland 1979; Coupland 1982] and Corti, *et al.* [Corti 1980] have reported that the addition of platinum (Pt) significantly improves environmental resistance in oxidizing and sulfidizing atmospheres. Pt also has the beneficial effect of partitioning to and stabilizing the γ' phase [Heidloff 2009; Van Sluytman 2010], thereby improving elevated-temperature strength. Despite such benefits, these materials pose significant challenges during thermomechanical processing (TMP) because of their narrow processing window in terms of acceptable flow stress and adequate hot workability.

II. Materials and Experimental Procedures

Two nickel-base superalloys, one with PGM alloying additions, were synthesized and processed to establish microstructure evolution during TMP. Initially, six 150-g buttons of each of two different aim compositions, Ni-15Al-5Cr-0.3Hf-0.25C-0.04B-0.04Zr (alloy "5A") and Ni-15Al-5Cr-3Pt-2Ir-0.3Hf-0.25C-0.04B-0.04Zr (alloy "5C") (in atomic percent), were vacuum arc-melted in the Materials Processing Laboratory at the Materials and Manufacturing Directorate of the Air Force Research Laboratory (Wright Patterson Air Force Base, OH). Each button was remelted three times to ensure homogeneous distribution of the alloying elements. Each group of six buttons was then remelted a fourth time and drop-cast into a water-cooled copper mold to produce a 25-mm diameter ingot at the DOE Ames Laboratory (Ames, Iowa).

The as-cast bars were hot isostatic pressed (HIP'ed) at a pressure of 207 MPa in an 8 hour cycle (including heating and cooling) reaching a maximum temperature of 1250°C to eliminate residual casting porosity. The HIP cycle was followed by a 42 hour homogenization heat treatment at 1250°C in air followed by water quenching. The γ' solvus temperature ($T_{\gamma'}$) was found to be ~1150°C for alloy 5A and ~1220°C for alloy 5C based on isothermal heat treatments performed in an inert argon atmosphere followed by water quenching.

Similar to conventional practices for superalloys, *supersolvus* hot working (at 1225°C) was used to breakdown the coarse structure of both alloys prior to machining performs for hot pack rolling. For this purpose, cylindrical samples measuring 25-mm diameter x 38-mm length were machined from the cast, HIP'ed, and homogenized bars and subjected to two series of four-hit compression deformations at a constant true axial strain rate of 10^{-2} s^{-1} with a 60 s dwell between each hit. During each hit, a true strain

increment of 0.2 was imposed, consistent with typical production cogging operations. The overall (total) true strain was thus 1.6. Following forging, the specimens were air cooled. Additional details regarding the hot compression experiments for alloys 5A [Pilchak 5A] and 5C [Ballard JECS] are reported elsewhere.

Rectangular preforms for flat rolling (largely at *subsolvus* temperatures) were extracted from the compressed cylinders of alloys 5A and 5C via wire electric-discharge machining (EDM). Each preform measured ~31 x 32 x 8.7 mm after light grinding to remove surface imperfections developed during the forging operation. Each perform was encapsulated in a can of proprietary design, preheated/reheated in indirect-resistance furnaces, and rolled on a two-high laboratory mill with 20-cm diameter, 30-cm wide rolls. Each pack was sufficiently thick and wide and the preform was sufficiently close to the midplane so that that the imposed deformation could be approximated as plane-strain compression.

Prior to rolling, each pack was preheated at 925°C for 20 minutes, transferred to a furnace at the nominal rolling temperature, and held for an additional 30 minutes. A range of rolling temperatures and total reductions (Table I) were utilized to gain a comprehensive perspective of band formation. Following preheating, all samples were rolled using a speed of 7.6 surface meters per minute (25 sfpm). An 8-pct. reduction was utilized for the first pass to seat the pack, followed by 12-pct. reduction on each subsequent pass. The rolling direction was reversed on each pass for unidirectionally-rolled specimens while the pack was rotated 90° between each pass for cross-rolled specimens. Furthermore, each pack was reheated between passes to restore the heat lost due to radiation and roll chill. Three-minute interpass reheats were utilized for the first 4 to 5 passes after which 2.5 minute interpass reheats were sufficient for the thinned material. Rolling to sheet consisted of approximately an 88 pct. total thickness reduction corresponding to a von Mises effective strain of ~2.4. Following the final pass, each pack was slow cooled in vermiculite and decanned. A one hour post-rolling flattening treatment was desirable upon reaching sheet gage. Initial flattening procedures (for samples 5C8-2R and 5C9-1XR, Table I) were performed at a high temperature (1163°C) (Table I). Subsequently, it was determined that lower temperatures produced acceptable flatness. Hence, the remaining flattening operations were performed at 704°C (5A3 specimens).

Preforms for foil rolling measuring ~32 x 37 x 1 mm were extracted from rolled-and-flattened sheets via wire EDM. The surfaces of the sheets were conditioned to remove imperfections in the as-rolled sheets which consisted of removing approximately 100 μm of material from both sides of the sheet. The exact amount of material removed was measured in each case, and was not included in the calculation of the total

reduction. The samples were then recanned, and subjected to multi-pass hot pack rolling with a target reduction of 75 pct., providing an additional true strain of 1.6. The 5A3 and 5C foils were given flattening treatments similar to the respective sheet materials.

Metallography was performed on sheet and foil rolled to total von Mises effective strains of approximately 1.04, 1.72, 2.4, and 4.2. To this end, specimens were sectioned from the sheet/foil with wire EDM or a slow-speed saw and mounted in conductive Bakelite. The mounts were ground successively using 320, 400, and 600 grit SiC papers followed by polishing with 9-μm, 6-μm, 3-μm, and 1-μm diamond paste with glycol-based extender. Final polishing was performed overnight using 0.05-μm non-crystallizing colloidal silica on a vibratory polisher. Scanning electron microscopy (SEM) and EBSD analysis were performed on samples in the as-polished condition using either an FEI Quanta 600 ESEM or an FEI XL30 ESEM (FEI Company, Hillsboro, OR), both of which were equipped with a field-emission gun. The accelerating voltage was 20 kV, and the probe current was approximately 10.5 nA.

III. Results and Discussion

The principal results from this research comprised the description of microstructure and texture during supersolvus breakdown of the cast microstructure and the (largely) subsolvus rolling to various levels of reduction for superalloys with or without PGM alloying additions. S*upersolvus* rolling was performed on one sample in order to understand how the presence of γ' affects microstructure and texture evolution during subsolvus rolling.

A. Microstructure Evolution during Hot Forging

Specimens were almost fully recrystallized following multi-hit supersolvus hot forging; however, coarse grains were periodically observed during backscattered-electron imaging. The unrecrystallized grains were elongated transverse to the compression direction. The fine, recrystallized grains had diameters between 100 and 200 μm (Figure 1). Flow curves measured during the multi-hit forging operation [Ballard JECS; Pilchak 5A] indicated that there was slight softening on successive hits, although nominally steady-state flow was achieved during each individual increment of strain. Thus, metadynamic recrystallization between hits was most likely the operative grain refinement mechanism as opposed to dynamic recrystallization. Because this was a multi-hit forging operation, however, some of the fine grains which were formed between early hits were subsequently deformed. In general, no further refinement was observed, but

orientation gradients present within some of the finer, recrystallized regions indicated that a geometrically-necessary dislocation substructure had developed within the recrystallized-and-deformed regions.

As deduced from large-area EBSD scans (Figure 2 and Figure 3) [Pilchak 5A], the unrecrystallized grains accounted for only a small fraction of the total microstructure (0.05 and 0.10 for alloys 5A and 5C, respectively). Two orientations seemed particularly difficult to recrystallize, namely, those with <100> and <110> parallel to the compression direction. The latter orientation has a high Taylor factor for axisymmetric compression (3.66) and, therefore, might be expected to be a difficult-to-work orientation. However, grains with <100> parallel to the compression direction have the lowest Taylor factor (2.45) and thus should be easily deformed. Indeed, the unrecrystallized regions observed in alloy 5C with <100> oriented nearly parallel to the compression direction contained orientation gradients indicating that they were deformed, but perhaps had not received sufficient strain to recrystallize.

The EBSD data also provided information regarding the texture (Figure 4), grain-size distribution (Figure 5a), and misorientation-angle distribution (Figure 5b) after hot compression. With regard to texture, both materials exhibited similar characteristics. However there were differences in the sharpness and intensity of the textures. For example, the non-PGM bearing alloy (5A) exhibited a sharp, well developed <100> partial fiber texture with the fiber axis parallel to the compression direction and a maximum intensity of ~6.1 times random. In contrast, the PGM alloy (5C) had apparently begun to develop the <100> fiber texture, but the density of {100} poles transverse to the compression direction varied between 0.5 and 3.0 times random along the fiber.

In order to make an appropriate comparison between the data from alloys 5A and 5C, the unrecrystallized regions were not included when calculating the grain-size and misorientation-angle distributions. Alloy 5C had a narrower distribution of grain sizes centered around 200 μm, while 5A had a wider distribution peaking at 350 μm. In addition, the largest grains in alloy 5C were ~ 500 μm while those in alloy 5A were more than twice that size. With regard to the misorientations, both alloys had strong peaks at 60° while the remainder of the distributions closely matched the Mackenzie behavior for randomly-oriented grains with cubic symmetry [Mackenzie 1958]. While some of the 60° misorientations can be associated with Σ3 twins, closer examination of the EBSD data sets (Figure 2 and Figure 3) revealed that the fraction of annealing twins was not large enough to account for the magnitude of the 60° peak. Additional effort is warranted to understand this observation.

B. Microstructure Evolution during Hot Pack Rolling

Due to the similar mechanisms operative during rolling of alloys 5A and 5C, microstructure and texture evolution as a function of imposed strain is described concurrently highlighted by representative examples from both alloys. While the rolling temperatures and overall reductions varied, the observations, taken together, provided a clear depiction of the sequence of microstructure evolution during hot pack rolling.

1. Macroscopic Strain ~ 1.04 (Total Reduction ~ 60 Pct.)

Rolling-direction inverse-pole-figure maps determined on longitudinal and transverse sections of alloy 5C after unidirectional rolling to a reduction of 60 pct. (sample 5C8-1R) are shown in Figure 6; in these maps, as well as all others depicting rolled sheet or foil, the rolling direction (RD) is horizontal for longitudinal sections. In this, and subsequent, data sets, black lines indicate a local pixel-to-pixel misorientation exceeding 5°, thereby defining a new "grain" for analysis purposes. The results in Figure 6 revealed that the sheet contained regions of similar orientation elongated in the rolling direction. These regions varied widely in size as well as aspect ratio; on average, they were 45-μm thick in the sheet normal direction (ND) with an aspect ratio (RD:ND) between 2:1 and 10:1. In general, thinner bands in the ND exhibited higher aspect ratios than the thicker ones. These features were also slightly elongated in the transverse direction (TD) as well. Postulating the conservation of grain volume (deduced from the grain area in two orthogonal sections), the sizes of these regions were consistent with flattening and elongation of grains in the starting structure. Furthermore, there were large orientation gradients within some of these regions, as evidenced by gradual changes in color within individual regions in both longitudinal and transverse sections of the sheet (Figure 6).

In addition to the high-aspect-ratio regions described above, several large bands were also observed that were between 100-μm and 300-μm thick (in the ND) and extended for one or more millimeters in the RD. Due to their larger size and infrequent appearance, these areas were most likely the result of further flattening and elongation of the small fraction of grains that had not been recrystallized during prior supersolvus hot compression. In the transverse section, two coarse bands were identified which both had 111 poles nearly parallel to the rolling direction with either {112} or {110} within ~10° of the rolling plane. The former orientation is close to the so-called 'copper' component of the FCC PSC deformation texture, while the latter is not considered to be stable with respect to the imposed deformation. The large bands observed in the longitudinal section were in orientations that more nearly corresponded to PSC deformation texture components. For example, the largest band in this image corresponded closely to the 'brass'

component, {110}<112>, in which {110} was precisely in the rolling plane, while <112> was between 5 and 20° from the rolling direction, depending on position along the band.

Aside from the coarse grains remnant from the double forged condition, approximately 35 pct. of the remaining bands were in orientations corresponding to one of the PSC deformation-texture components (Table II, column for 5C8-1R). As mentioned above, the elongated bands contained large orientation gradients, and thus in many cases only part of a given band actually exhibited a stable deformation-texture component while the remaining portion seemed to be rotating toward this orientation, but the imposed strain was insufficient to fully reorient the lattice of the entire band.

Physically, orientation gradients within a band must be accommodated by geometrically-necessary dislocations. High-resolution EBSD quantified this behavior (Figure 7). For example, a rolling-direction inverse-pole-figure map (Figure 7a) revealed the wide range of lattice orientations contained within individual grains. A gray-scale image-quality parameter in conjunction with orientation coloring more clearly distinguished the cell/subgrain boundaries within grains (Figure 7b). This image clearly showed that there is a preferred alignment of cells/subgrains at approximately 30° to the RD in the central grain. However, the traces of these features do not align with any low-index crystallographic plane. In Figure 7c, the boundaries between adjacent pixels with misorientations of various degrees have been delineated. These data showed that there was substantially more substructure developed within the central grain compared to that in adjacent grains. In addition, the continuous networks of blue lines at the boundaries of the highly-misoriented bands indicated that these were likely preferential nucleation sites for metadynamic (or static) recrystallization between passes. There is also some evidence of grain nucleation inside the central band, but this location is clearly less favored. Based on the continuous gradients in color leading up to these nuclei, they are presumably formed by a continuous dynamic recrystallization mechanism in which sub-boundaries form and rotate progressively until becoming mobile at a high enough misorientation (> 15°, for instance). This point is addressed in more detail later.

It is interesting to note that the majority of the central grain did not correspond to one of the stable deformation-texture components, although some of its subgrains had rotated into the characteristic S1 or S2 orientations (Figure 7d). On the other hand, the orientations of the grains at the top left and bottom of the images corresponded to the S2 and S3 orientations, respectively, and neither exhibited substantial subgrain formation implying that subgrain formation is not necessary as grains rotate toward stable orientations. However, the band with red and orange hues in the inverse-pole-figure map (Figure 7a), lying

just above that in the S3 orientation, was not in a stable deformation-texture orientation nor did it exhibit significant subgrain formation implying that this phenomenon is strongly dependent on orientation.

2. Macroscopic Strain ~ 1.72 (Total Reduction ~ 77.5 Pct.)

After 77.5-pct. thickness reduction at a *supersolvus* temperature, the microstructure consisted primarily of elongated bands that were again made up of continuous orientation gradients (sample 5A1-1R, Figure 8). In general, the boundaries between adjacent bands were more nearly perpendicular to the sheet normal direction than in specimens rolled to 60 pct. reduction. The interfaces were not necessarily flat along the entire length of the band, but showed some degree of curvature. At this level of deformation, however, the bands were too thick in the sheet normal direction and too long in the rolling direction to correlate to recrystallized grains present after hot compression which had been flattened and elongated by rolling. In addition, the large volume fraction of these bands made it impossible for them to have originated solely from grains that were not recrystallized following hot compression. The formation of elongated bands in the absence of γ' suggests that the presence of heavy solute elements in the program alloys, like platinum and iridium, are sufficient to inhibit classical discontinuous dynamic recrystallization, or static recrystallization during interpass reheating. The effect of the solutes can also be observed in the grain size distributions in Figure 5a. The non-PGM bearing alloy, 5A, achieves a substantially larger mean grain size compared to alloy 5C during supersolvus forging. However, as discussed by Semiatin et al. [Semiatin 1991], temperature transients exist during high temperature pack rolling as the pack is transferred from the furnace to the mill and also due to roll chill, although heat loss during the former is greater. Initially, the pack was 16.4 mm thick and the rolling furnace was maintained 40 °C above the γ' solvus temperature so the pack was most likely rolled supersolvus. However, the pack was only 3.25 mm thick on the final pass which could have resulted in more significant heat loss during transfer allowing some γ' to precipitate and affect microstructure evolution.

Using data from an area approximately five times larger than that shown in Figure 8 to provide a statistically relevant estimate, only 35 pct. of the grains in this sample were within 10° of a typical deformation-texture component for PSC (Table II, sample 5A1-1R). It was found that bands in the cube orientation, accounting for approximately 10 pct. of the total sample, were the most frequently observed. Other than the cube-oriented bands, the three S components and the Taylor orientation were most prominent at this level of reduction; this latter finding may be related perhaps to the multiplicity of the S and Taylor orientations because they are not composed of low-index planes and directions and thus would be statistically more

likely to occur as grains are rotating toward other stable texture components. In addition, several bands were observed to shift from one deformation texture component to another along the length of the band. This was most frequently observed in bands with the S orientations, which tended to vary between S1, S2, and S3. This result is not unexpected, however, as the S orientations lie very close to one another in orientation space.

3. Macroscopic Strain ~ 2.4 (Total Reduction ~ 88 Pct.)

Reductions of approximately 88 pct. served as an intermediate step for rolling to 250-μm thick foil [Ballard JECS]. Thus, many samples had been deformed to this level using both unidirectional and cross rolling (Table I). As mentioned previously, flattening of 5C sheet was performed at 1163°C, thus altering the microstructure so that it was no longer appropriate to characterize it as being "as-rolled". Thus, in order to understand microstructure evolution throughout the entire sequence of processing steps, specimen 5A3-1R was investigated in detail at each step of the process and is described in detail in subsequent subsections followed by a brief comparison with 5C8 and 5C9 samples. It should also be borne in mind that the packs were slow cooled in vermiculite after rolling, and therefore the observed microstructures may have experienced some metadynamic recrystallization. Roll chill experienced during the final pass at which the pack is thin, the presence of primary γ', and the precipitation of secondary γ' during cooling would all tend to limit such microstructure changes, however. Moreover, based on the results from the preceding sections, it is clear that the features of primary interest (the unrecrystallized bands) were formed *during* rolling.

<u>As-Rolled Condition.</u> EBSD analysis of the as-rolled sheet revealed that approximately 85 pct. of the microstructure was composed of elongated bands with well-defined interfaces parallel to the rolling plane. The remaining 15 pct. consisted of fine, recrystallized grains that were primarily located at the interfaces between highly misoriented bands, although a small fraction of what appeared to be recrystallization nuclei were present *within* some bands. Inverse-pole-figure and PSC texture-component maps (Figure 9, Table II) illustrate these observations. For example, fine, equiaxed grains are seen above and below the large {110}<112>-oriented band extending across the middle of the image. In some cases, these equiaxed grains appear to have recrystallized into other PSC deformation-texture components, including Taylor and copper orientations indicated by light blue and orange hues, respectively. By contrast, highly-misoriented subgrains (> 15°) which do not coincide with any ideal PSC texture component were found within the elongated bands (Figure 9, arrows). The fraction of these features, which may represent nuclei for discontinuous recrystallization, was small compared to those at the boundaries between highly misoriented bands. There

was no evidence of particle-stimulated nucleation due to coarse primary γ' or carbide phases. In fact, the presence of primary γ' in conjunction with slow diffusing solutes likely inhibited grain boundary migration, thereby retaining major features of the deformation texture despite the large imposed strains.

Although it is not obvious in the inverse-pole-figure map (Figure 9a), the PSC texture-component map (Figure 9b) indicated that the {110}<112>-oriented band formed several narrow regions of the S3 orientation that were elongated in the rolling direction. This observation appears to be direct evidence for the band-splitting phenomenon described by Maurice and Driver [Maurice 1993; Maurice 1997a] and Samajdar and Doherty [Samajdar 1998]. This point, along with a description of a possible mechanism for the formation of new bands, is addressed in more detail below.

Rolled-and-Flattened Condition. After the low temperature flattening processes given to the sheets rolled from alloy 5A, the microstructure consisted of only a slightly smaller area fraction of banded grains than in the as-rolled condition; i.e., ~80 pct. compared to 85 pct. in the as-rolled condition. The reduction of total band area was due to additional recrystallization occurring at the interfaces between highly misoriented bands as described previously. Subgrain evolution was also investigated by comparing the misorientation distributions of individual bands of the same orientation in the as-rolled condition with the flattened condition. No statistically significant changes were observed indicating that the flattening procedure did not alter the microstructure at the constituent level.

Band Splitting. While some evidence of band splitting had been noted in sample 5A3-1R (Figure 9), observations for sample 5A1-2R provided clearer insight into the mechanism by which it occurs. The latter specimen was rolled from an initial condition already containing a banded microstructure (Sample 5A1-1R, Table I, Figure 8). Examination of the microstructure after rolling (Figure 10a) revealed that almost the entire sample consisted of unrecrystallized bands with minimal recrystallization occurring during deformation or cooling. However, following the second rolling campaign, only 48 pct. of the bands in this sample were within 10° of an orientation corresponding to a PSC ideal deformation-texture component. This amount is only somewhat greater than the ~ 35 pct. found after the first rolling campaign despite an additional strain increment of 0.7. The most favored orientations were the S1, S3, and Taylor. Furthermore, the fraction of cube-oriented bands was reduced by a factor of two compared to the initial (5A1-1R) condition. Close inspection of the cube-oriented bands near the top and bottom of sheet 5A1-1R (Figure 8) revealed evidence of shear bands like those described by Sokolov, *et al.* [Sokolov 2005]. In this case, the shear bands were restricted to an individual elongated band and did not cross the boundary with adjacent

elongated grains. Moreover, gradients of red and orange hues noted in the inverse-pole-figure map represent cube and non-cube oriented regions, respectively (Figure 8). In the accompanying texture-component map, these correspond with red and white regions, respectively, indicating that the shear bands may be rotating regions of the bands away from the cube orientation even at the moderate level of strain imposed to specimen 5A1-1R.

A high resolution EBSD scan from specimen 5A1-2R (Figure 10b) showed a location in which a thin purple band appeared to have formed from a host band in a completely different orientation. Intersecting shear bands lying at 45° to the rolling plane were evident within the host band. Dislocation motion is essential for shear band formation and dislocations inherently produce lattice rotations in constrained crystals [Kocks 1998]. Thus, material elements lying within the shear bands are continuously rotated as strain is accumulated. On the other hand, material elements lying at the intersection of two (orthogonal) shear bands may represent a special case in which a shape change can occur (e.g., a narrowing of an unrecrystallized band in the ND and elongation in RD) without the need for lattice rotation [Kocks 1998]. In polycrystals, this is virtually impossible to achieve inasmuch as heterogeneous strain accumulation caused by local neighborhood effects ultimately causes one slip system to be favored over the other resulting in a net lattice rotation within unrecrystallized bands.

In the present case, the shear bands gave rise to continuous lattice rotations that resulted in the formation of a new band consisting of the S1 and S3 orientations contained within an outer layer of S2 (Figure 10c). Presumably, the S2 orientation served as a transition point to the other orientations as it lies between them in the orientation distribution. Transition bands of this nature have also been reported in the past by Maurice and Driver [Maurice 1993]. The orientations belonging to the rotated cube and newly-formed S-oriented bands were extracted from the data set and used to generate the pole figures in Figure 11. There was a large spread in orientations within the host band (~25°) due to the presence of subgrains; the spread was reduced as the S orientations were approached. These pole figures suggest that the new band is formed by the continuous rotation of subgrains and not by a *discontinuous* dynamic recrystallization mechanism in which highly-misoriented (subgrain) nuclei form and migrate into the surrounding matrix. The average orientation of the host band was a rotated cube with <001> essentially parallel to the rolling direction, but the orthogonal <100> was tilted ~ 25° from ND giving this band a low Taylor factor, ~2.4, (Figure 11d). In contrast, the newly formed band had a considerably *higher* Taylor factor (~3.3). Therefore,

the formation of the new band was not due to texture softening which could drive the localization of strain and hence the formation of shear bands.

In addition to causing lattice rotations leading to a new texture-component via continuous dynamic recrystallization, the shear bands appeared to serve another important purpose; i.e., the nucleation of new orientations. Specifically, while the interfaces between any two highly misoriented, unrecrystallized bands appeared flat at the macroscopic scale (Figure 10a), higher resolution images (Figure 9 and Figure 10b) revealed that the interfaces actually exhibited significant local deviations. These "jagged" features, previously identified as favored nucleation sites, appear to be formed when shear bands within an unrecrystallized band intersected the interface between this band and its neighbor. The high local strains and high boundary curvature thus created at these locations appeared to be potent nucleation sites for *discontinuous* dynamic/metadynamic recrystallization based on the observation of recrystallized grains at these locations in the as-rolled condition. In this regard, Canova, *et al.* [Canova 1984] described a similar situation in which shear band formation in one grain destroyed the planarity of its interface with the adjacent grain. However, the authors also suggested that this resulted in a relaxed-constraints condition which could stimulate shear-band formation in the adjacent band.

The lattice rotations around a stable orientation noted in the present work provide further insight into band-splitting phenomena discussed by others. For example, Zhou, *et al.* [Zhou 1992] investigated the stability of the ideal orientations during rolling using a rate-sensitive crystal-plasticity analysis assuming {111}<110> restricted slip under full constraints and two types of relaxed-constraints conditions. They analyzed the results in terms of the three dimensional lattice-rotation velocity fields as well as the gradients and divergence around the locations of the ideal orientations in Euler space. In the relaxed constraints model simulating "pancake compression", also known as the flat grain limit [Kocks 1998], the results showed that no orientations are truly stable, but that orientations flow into and out of the "stable" positions on the α- and β-fibers of the FCC rolling texture [Zhou 1992; Kocks 1998]. The three-dimensional lattice rotation fields are particularly useful inasmuch as they showed that small deviations from the ideal orientations can result in high rates of lattice rotation away or toward other positions on the α- and β- fibers. This is particularly true for the S and brass orientations, but not for the cube orientation. The rate of rotation away from cube is small initially, but increases as the grain becomes further misoriented from the perfect cube location. Thus, cube bands may require larger lattice rotations (e.g., due to shear band formation) in order to split.

4. Macroscopic Strain ~ 4.2 (Total Reduction ~97 Pct.)

Relatively uniform foil thicknesses between 180 μm and 250 μm were achieved by hot-pack-rolling. Thickness variations over the entire length of the foils were generally less than 15 μm. In alloy 5C, which was rolled to a strain of 4.17, the banded microstructure was completely eliminated by rolling to foil and the resultant microstructure consisted of equiaxed γ grains ~20 μm in diameter and globular γ' precipitates (Figure 12). The majority of γ' was incoherent with respect the γ phase indicating that it was present during rolling and may have acted to inhibit recrystallization and grain growth during interpass reheating. In addition, many of the γ grains contained annealing twins that formed presumably during the interpass reheats or cooling from the rolling temperature. In alloy 5A, which was rolled to a true strain of ~4.21, the microstructure was almost fully recrystallized, although some remnants of elongated, cube-oriented bands were observed which constituted ~7 pct. by area of the total microstructure. Recrystallized grains grew into the cube-oriented bands, thus severing them such that the bands were discontinuous. In general, the unrecrystallized cube-oriented regions were 30 μm in the rolling direction and ~5 μm in the sheet-thickness direction. The presence of bands in alloy 5A, but not in alloy 5C, is most likely related to the difference in rolling temperature.

Although uniform foil thickness was achieved while maintaining fine grain size, small cavities were observed at γ/γ and γ/γ' boundaries in the rolled-and-flattened foils (Figure 13). Because these materials are being developed for non-load bearing applications, the impact on the service performance of such non-surface-connected cavities is not clear. In this context, however, it is noteworthy that commercially-available sheet and foil of Haynes® 230® (Haynes International, Kokomo, IN) contains stringers of fractured carbides with voids around them. This alloy exhibits excellent oxidation resistance at high temperature and thus is used for applications similar to those intended for the present program alloys.

5. Cross-Rolled PGM-Modified Alloy

The evolution of microstructure in the PGM-modified alloy *cross rolled* to sheet was similar to the results for unidirectionally-rolled sheet samples described above. However, the remnant banded regions were generally two to three times *thicker* (in the sheet ND) than in samples unidirectionally rolled to the same level of effective strain (Figure 14) despite the fact that the cross-rolled samples were given an additional one-hour flattening/static recrystallization heat treatment at the rolling temperature. In addition to being thicker in the ND, the bands in the cross-rolled material were in effect "infinite sheets" in the rolling plane, being approximately the same dimension in both rolling directions. This is in contrast to the narrow "slabs" observed in the unidirectionally rolled material; i.e., these bands were one-quarter to one-half the size in the

TD compared to RD. The larger size of the bands and their persistence after high temperature flattening suggested that the bands stored a smaller amount of work during cross-rolling compared to that developed/stored during unidirectional rolling.

While the banded microstructure was completely eliminated by unidirectional rolling to foil (~97 pct. reduction, von Mises effective strain ~4.17), a single cube-oriented band persisted near the center of the cross-rolled PGM material even after the high temperature, one-hour flattening/recrystallization treatment. A portion of the band is shown in Figure 15. Data acquired from a much larger area (~3 mm long) indicated that the band was approximately 2 mm long and had a uniform thickness of ~ 5 μm.

V. Summary and Conclusions

The formation of a banded structure during hot pack rolling of nickel-base superalloys was quantified using electron backscatter diffraction (EBSD). The results demonstrated that the elongated, unrecrystallized bands are formed by slip-induced lattice rotations that move grains toward stable orientations with respect to the imposed plane-strain compression. At small reductions, the overall shape of each elongated band can be rationalized in terms of flattening in the ND and elongation in the RD of the grains present in as-forged material. Upon reaching larger strains, on the other hand, the total number of bands is reduced and they are sufficiently large that they can no longer be accounted for by a conservation-of-volume argument. Furthermore, while approximately 85 pct. of the microstructures of as-rolled sheets comprised unrecrystallized bands, only 35 pct. to 50 pct. were within 10° of a stable texture component. These observations, combined with the fact that many of the bands exhibited large, continuous orientation gradients spanning multiple texture components, suggested that the larger bands formed when groups of grains rotated toward the same texture component. This conceptual mechanism can also be used to understand the formation of orientation gradients along the RD within the bands. The rate of rotation toward (or away from) a given orientation for a specified macroscopic deformation is not a constant, but rather changes for each initial orientation. Thus, bands formed from grains in initially different orientations would tend to maintain orientation gradients along their length because not all initial grains reach the ideal (stable) orientation at the same strain. High-resolution EBSD analysis also demonstrated unambiguously that upon reaching a stable orientation, shear-band formation within an unrecrystallized band may lead to local lattice rotation away from the ideal component thus forming a band of a new orientation. A region of continuous lattice rotation was observed between the unrecrystallized band and the newly formed band indicating that this was most likely due to a continuous dynamic recrystallization process and not due to discontinuous

dynamic recrystallization or classical static recrystallization. Persistence of the banded microstructure during *supersolvus* rolling suggested that solute drag due to the presence of slow diffusing elements like platinum and iridium was sufficient to inhibit discontinuous dynamic recrystallization in the absence of pinning particles of primary γ'.

Acknowledgements

This work was conducted as part of the in-house research activities of the Metals Processing Group of the Air Force Research Laboratory's Materials and Manufacturing Directorate. The support and encouragement of the Laboratory management and the Air Force Office of Scientific Research (Dr. Ali Sayir, program manager) are gratefully acknowledged. The authors also wish to acknowledge T. Brown, J. Brown, and T. Goff for performing the hot-pack-rolling trials. One of the authors (ALP) was supported through AFOSR Contract FA8650-07-D-5800.

References

[Necker 1997] C.T. Necker: Recrystallization texture in cold rolled copper, PhD Dissertation, Drexel University, 1997.

[Samajdar 1998] I. Samajdar and R.D. Doherty: Cube recrystallization texture in warm deformed aluminum: understanding and prediction, Acta Mater., 46, 1998, pp. 3145-3158.

[Caleyo 2001] F. Caleyo, T. Baudin, R. Penelle, and V. Vengas: EBSD study of the development of cube recrystallization texture in Fe-50%Ni, Scripta Mater., 45, 2001, pp. 413-420.

[Sokolov 2005] B.K. Sokolov, I.V. Gervas'eva, D.P. Rodionov, Yu.V. Khlembikova, L.R. Vladimirov, and R.A. Schwartser, The Physics of Metals and Metallography, 99;2, 2005, pp. 172-182.

[Canova 1984] G.R. Canova, U.F. Kocks, and M.G. Stout: On the origin of shear bands in textured polycrystals, Scripta Metall., 18, 1984, pp. 437-442.

[Park 1997] L.-J. Park, J.H. Tundermann, and J.J. deBarbadillo: Scripta Materialia, 37;12, 1997, pp. 1995-2001.

[Lee 1999] J.-H. Lee, L.-J. Park, S.-N. Kim, and K.-W. Paik: J. Mater. Sci. Letters, 18, 1999, pp. 1645-1648.

[Hirsch 1988] J. Hirsch and K. Lucke: Acta Metall., 36, 1988, pp. 2863.

[Humphreys book] F.J. Humphreys and M. Hatherly: Recrystallization and Related Annealing Phenomena 2nd ed., Elsevier, Kidlington, Oxford, UK, 2004.

[Ballard JECS] D.L. Ballard, D.S. Weaver, A.L. Pilchak, and S.L. Semiatin: Hot Working of Platinum Group Metal-Modified Ni-Base Superalloys for Thermal Protection System Applications, J. Eur. Ceramic Soc., 20101, in press.

[Coupland 1979] D.R. Coupland, C.W. Corti, and G.L. Selman: The PGM concept: Enhanced corrosion resistant superalloys for industrial and aerospace applications, Proceedings of the Pettern Int'l. Conf. on the Behaviour of High Temperature Alloys in Aggressive Environments, 1979.

[Coupland 1982] D.R. Coupland, C.W. Hall, and I.R. McGill: Platinum-enriched superalloys - A developmental alloy for use in industrial and marine gas turbine environments, Platinum Metals Rev., 1982, 26, pp. 146-157.

[Corti 1980] C.W. Corti, D.R. Coupland, and G.L. Selman: Platinum-enriched superalloys - Enhanced oxidation and corrosion resistance for industrial and aerospace applications, Platinum Metals Rev., 1980, 24, pp. 2-11.

[Heidloff 2009] A.J. Heidloff, J. Van Slutyman, T.M. Pollock and B. Gleeson: Structural stability of platinum-group-metal-modified $\gamma + \gamma'$ Ni-base alloys, Metall. Mater. Trans. A, 40A, 2009, pp. 1529-1540.

[Van Sluytman 2010] J.S. Van Sluytman, A. La Fontaine, J.M. Cairney, and T.M. Pollock: Elemental partitioning of platinum group metal containing Ni-base superalloys using electron microprobe analysis and atom probe tomography, Acta Mater., 58, 2010, pp. 1952-1962.

[Pilchak 5A] A.L. Pilchak, D.S. Weaver, D.L. Ballard, and S.L. Semiatin: Grain refinement during hot compression of a Ni-base superalloy, in preparation.

[Mackenzie 1958] J.K. Mackenzie: Second paper on statistics associated with the random disorientation of cubes, Biometrika, 45, 1958, pp. 229-240.

[Semiatin 1991] S.L. Semiatin, M. Ohls, and W.R. Kerr: Scripta Metall. et Mater., 25, 1991, pp. 1851-1856.

[Doherty 1997] R.D. Doherty, D.A. Hughes, F.J. Humphreys, J.J. Jonas, D. Juul Jensen, M.E. Kassner, W.E. King, T.R. McNelley, H.J. McQueen, and A.D. Rollet: Current issues in recrystallization: A review, Mat. Sci. Eng. A, 238, 1997, pp. 219-274.

[Kocks 1998] U.F. Kocks, C.N. Tomé , and H.-R. Wenk: Texture and Anisotropy: Preferred Orientations in Polycrystals and their Effect on Materials Properties, Cambridge University Press, New York, NY, 1998, pp. 328-330.

[Zhou 1992] Y. Zhou, L.S. Toth, and K.W. Neale: On the stability of the ideal orientations of rolling textures for fcc polycrsytals, Acta Metall. Mater., 40, 1992, pp. 3179-3193.

Table I. Hot-Pack-Rolling Parameters*

Sample Designation	Initial Condition	Rolling Furnace Temperature** (°C)	Total Rolling Reduction (Pct.) / Effective Strain***	Final Thickness (mm)
5A1-1R	Double forged	1190	77.5 / 1.72	1.816
5A1-2R	5A-1-1R	1130	87.4 / 2.4	1.016
5A3-1R	Double forged	1130	88.2 / 2.47	0.991
5A3-2R	5A3-1R	1135	97.4 / 4.21	0.171
5C8-1R	Double forged	1190	59.4 / 1.04	3.556
5C8-2R	5C8-1R	1190	88.0 / 2.45	1.130
5C8-3R	5C8-2R	1190	97.3 / 4.17	1.842
5C9-1XR	Double forged	1190	89.0/ 2.56	1.041
5C9-2XR	5C9-1XR	1190	96.1 / 3.75	0.171

*All samples were unidirectionally rolled except 5C9-1XR and 5C9-2XR.
**γ'-solvus temperatures of the program alloys were 1150°C (alloy 5A) and 1220°C (alloy 5C).

Table II. Fraction of Deformation Texture Components (with a 10° Tolerance*) in the As-Hot-Pack-Rolled Condition (Prior to Flattening)**

Legend	Texture Component	Miller Indices	Specimen ID / Fraction of Each Component			
			5A1-1R	5A1-2R	5A3-1R	5C8-1R
	Copper	{112}<111>	0.007	0.035	0.019	0.025
	S1	{124}<211>	0.086	0.144	0.077	0.088
	S2	{123}<412>	0.030	0.032	0.039	0.042
	S3	{123}<346>	0.039	0.076	0.107	0.050
	Taylor	{4 4 11}<11 11 8>	0.062	0.095	0.025	0.045
	Brass	{110}<112>	0.021	0.044	0.067	0.068
	Goss	{110}<001>	0.009	0.002	0.006	0.016
	Cube	{001}<100>	0.098	0.052	0.116	0.021
		Total:	0.352	0.48	0.456	0.355

* Each PSC texture-component color fades to white over an angular range of 10° from the ideal orientation.
**The color legend shown here is identical to that used in the plane-strain-compression texture-component maps.

Figure Captions

Figure 1. Representative backscattered electron image of the microstructure of alloy 5A after supersolvus double forging.

Figure 2. Compression- and normal-direction inverse-pole-figure maps of alloy 5A following double forging.

Figure 3. Compression-direction inverse-pole-figure map of alloy 5C following double forging.

Figure 4. Texture of the as-double forged materials. The compression direction (z) is vertical in order to be consistent with the data in Figure 2 and Figure 3.

Figure 5. (a) Grain size and (b) misorientation-angle distributions for alloys 5A and 5C after hot compression.

Figure 6. Longitudinal- and transverse-section inverse-pole-figure maps for the rolling direction of sample 5C8-1R. (Although the two sections are orthogonal to each another, the orientations have been colored in both cases relative to the rolling direction (horizontal for the longitudinal section and into the plane of the image for the transverse section).

Figure 7. (a) Rolling-direction inverse-pole-figure map, (b) same as (a) with an image quality grayscale map applied, (c) color-coded grain-misorientation map (pixel-by-pixel method), and (d) PSC texture component map from sample 5C8-1R (see Table I for legend).

Figure 8. Rolling-direction inverse-pole-figure map and rolling-texture-component map for sample 5A1-1R.

Figure 9. Rolling direction inverse-pole-figure map and rolling-texture-component map of as-rolled 5A3-1R. The arrows indicate highly-misoriented subgrains within the {110}<112> (copper) oriented band.

Figure 10. (a) Rolling-direction inverse-pole-figure-map, (b) higher resolution scan of the region enclosed by the black box in (a), (c) deformation-texture-component map, and (d) Taylor-factor map for sample 5A1-2R.

Figure 11. Discrete equal-angle pole figures showing the continuous nature of the evolution of a near-cube oriented band into the S3 orientation in sample 5A1-2R.

Figure 12. Rolling-direction inverse-pole-figure map of sample 5C8-3R.

Figure 13. Backscattered electron image of rolled-and-flattened sample 5C8-3R. The red circles indicate voids at γ/γ grain boundaries; blue circles indicate voids at γ/γ' boundaries.

Figure 14. Rolling-direction inverse-pole-figure map of sample 5C9-1XR with image-quality overlay.

Figure 15. Rolling-direction inverse-pole-figure map of specimen 5C9-2XR.

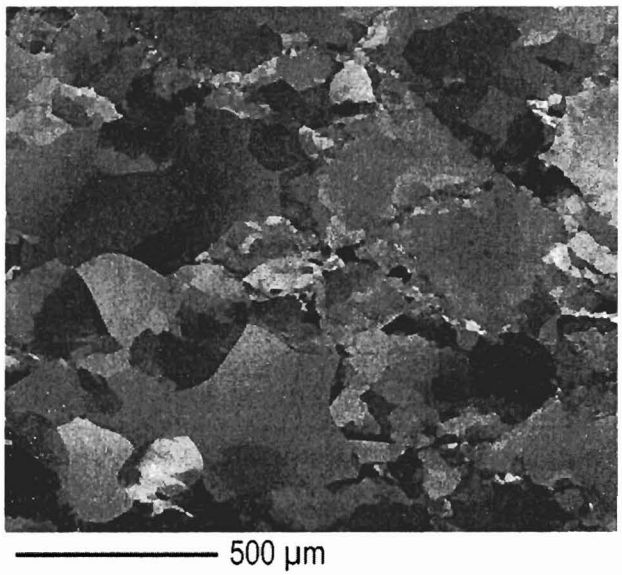

Figure 1. Representative backscattered electron image of the microstructure of alloy 5A after supersolvus double forging.

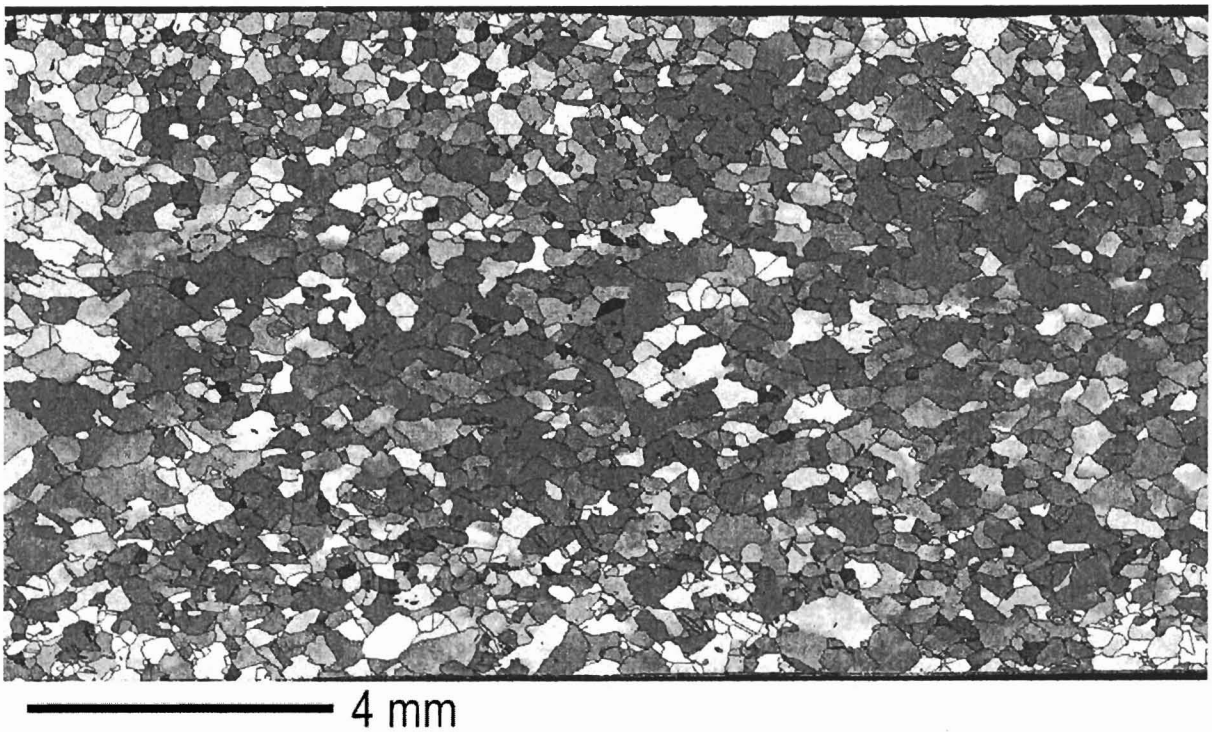

Figure 2. Compression-direction inverse-pole-figure maps of alloy 5A following double forging.

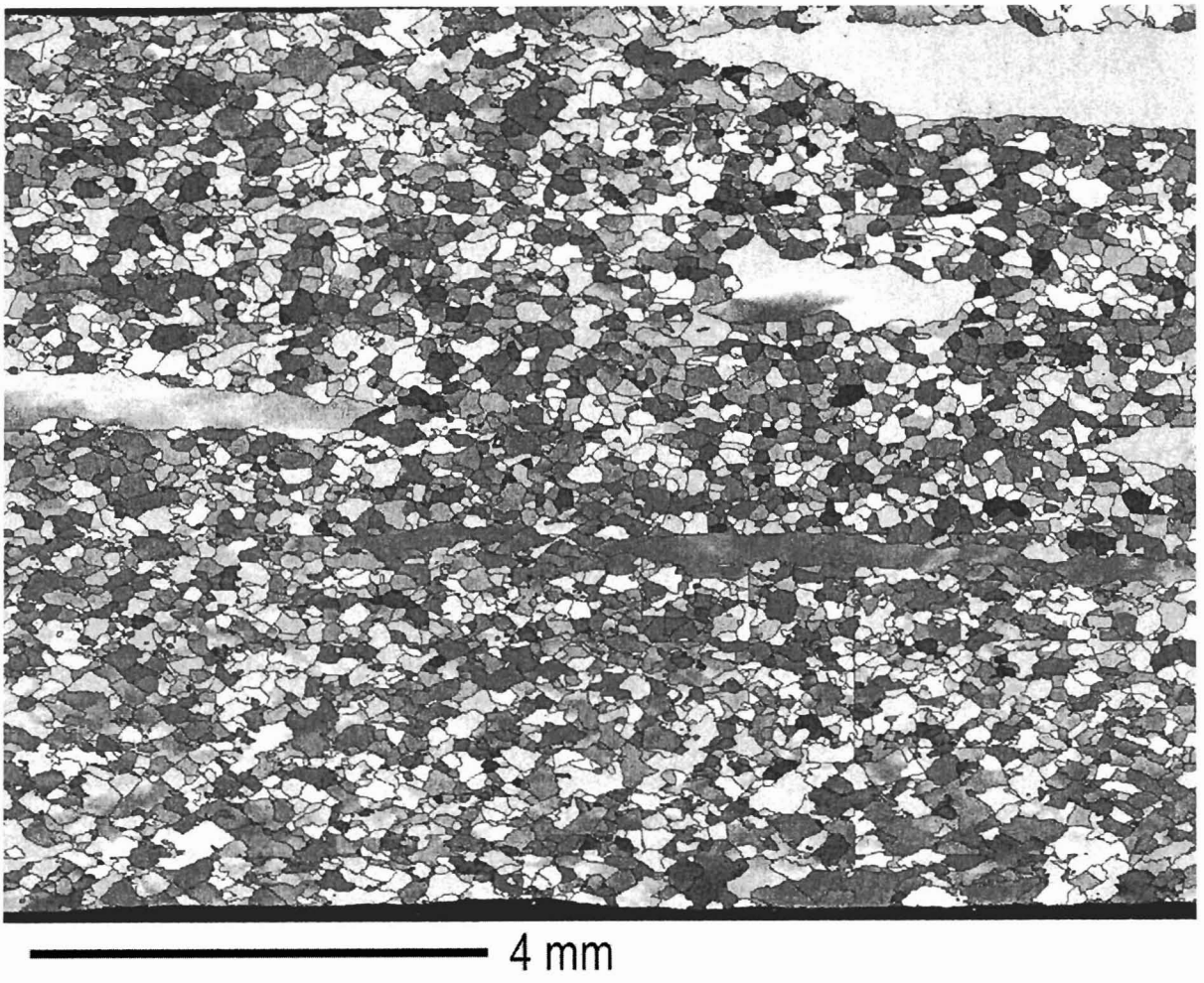

Figure 3. Compression-direction inverse-pole-figure map of alloy 5C following double forging.

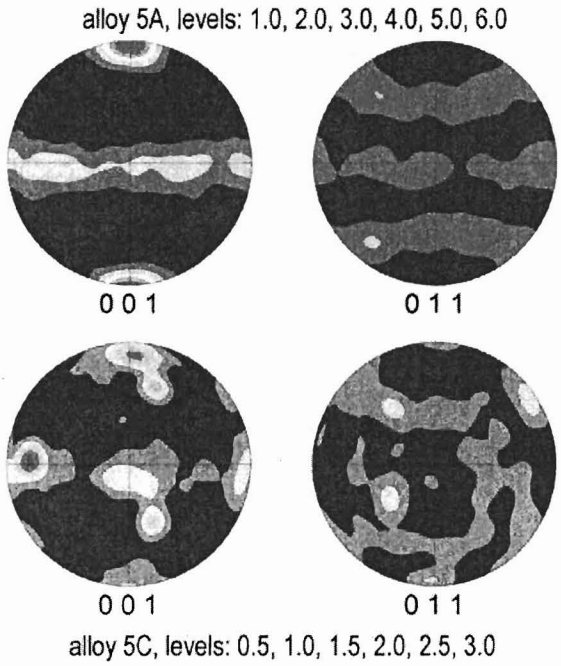

Figure 4. Texture of the as-double forged materials. The compression direction (z) is vertical in order to be consistent with the data in Figure 2 and Figure 3.

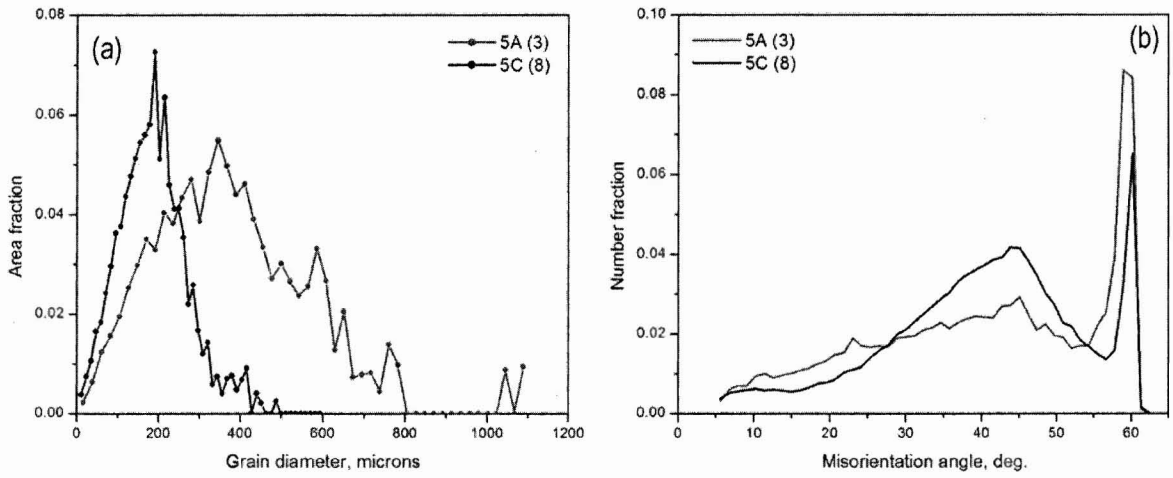

Figure 5. (a) Grain size and (b) misorientation-angle distributions for alloys 5A and 5C after hot compression.

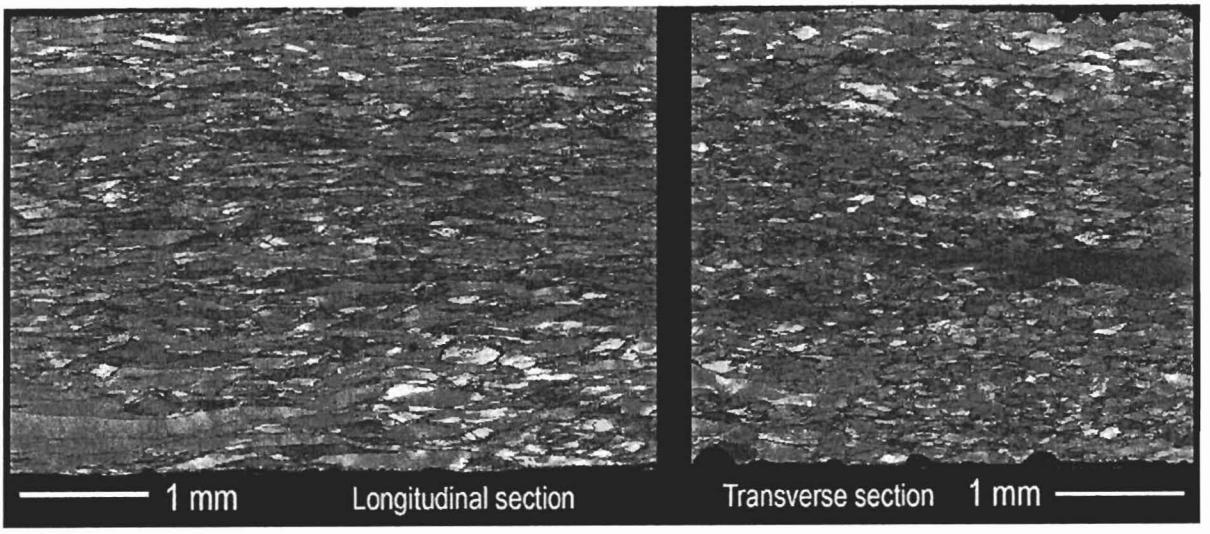

Figure 6. Longitudinal- and transverse-section inverse-pole-figure maps for the rolling direction of sample 5C8-1R. (Although the two sections are orthogonal to each another, the orientations have been colored in both cases relative to the rolling direction (horizontal for the longitudinal section and into the plane of the image for the transverse section).

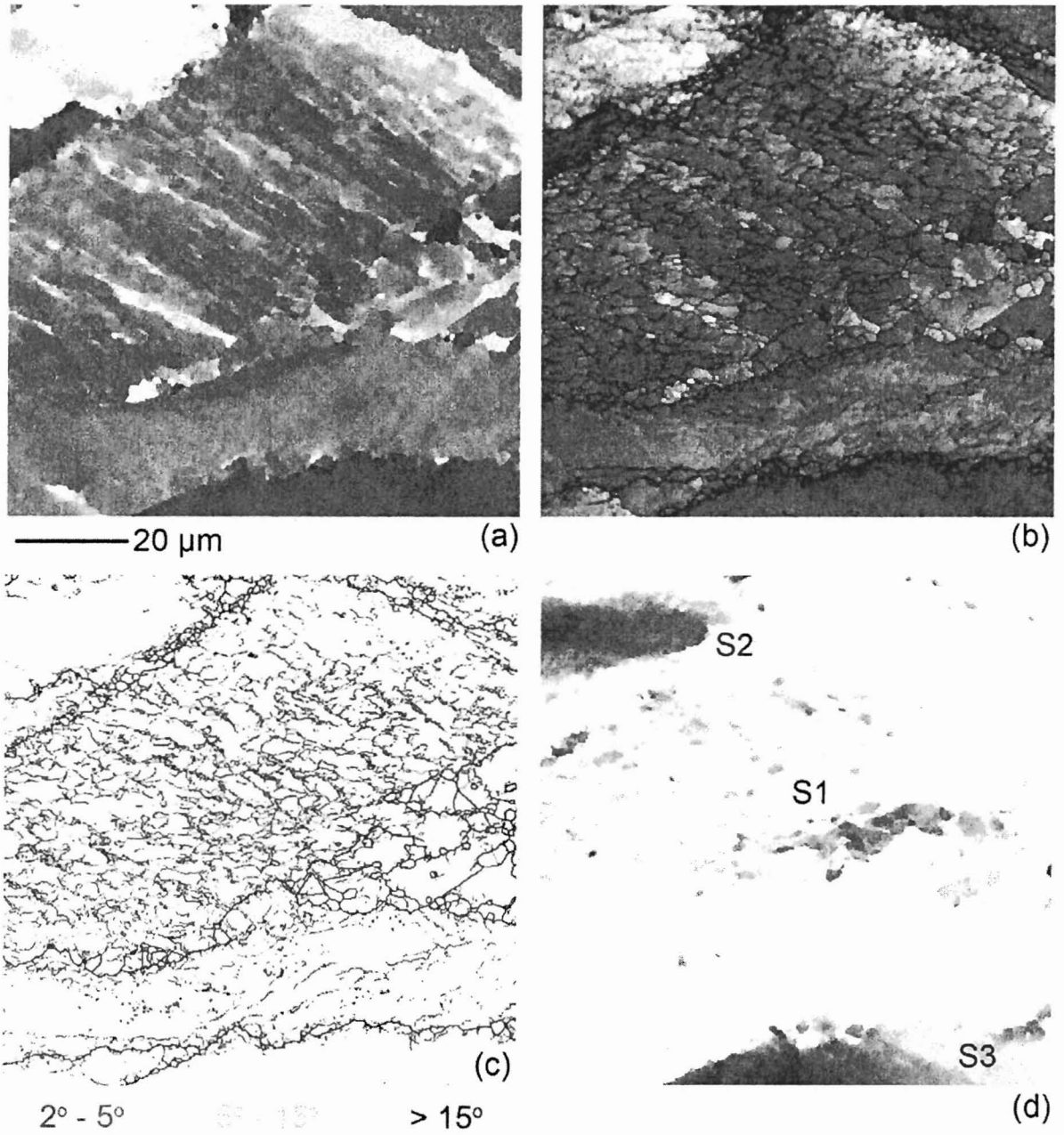

Figure 7. (a) Rolling-direction inverse-pole-figure map, (b) same as (a) with an image quality grayscale map applied, (c) color-coded grain-misorientation map (pixel-by-pixel method), and (d) PSC texture component map from sample 5C8-1R (see Table I for legend).

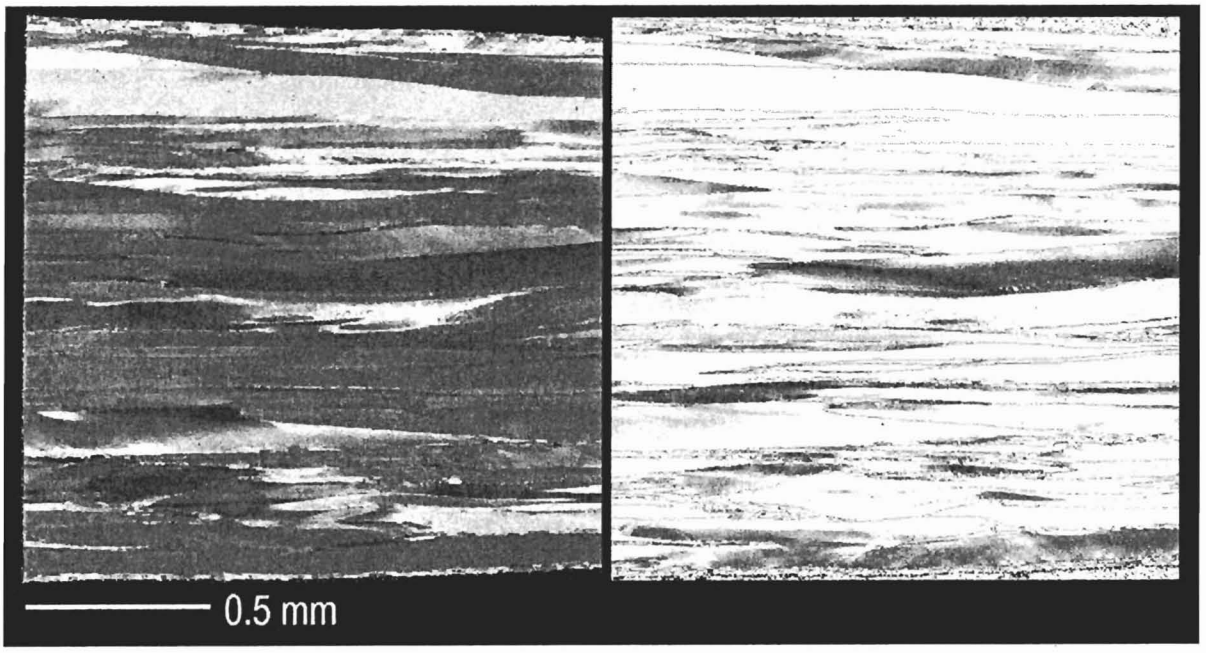

Figure 8. Rolling-direction inverse-pole-figure map and rolling-texture-component map for sample 5A1-1R.

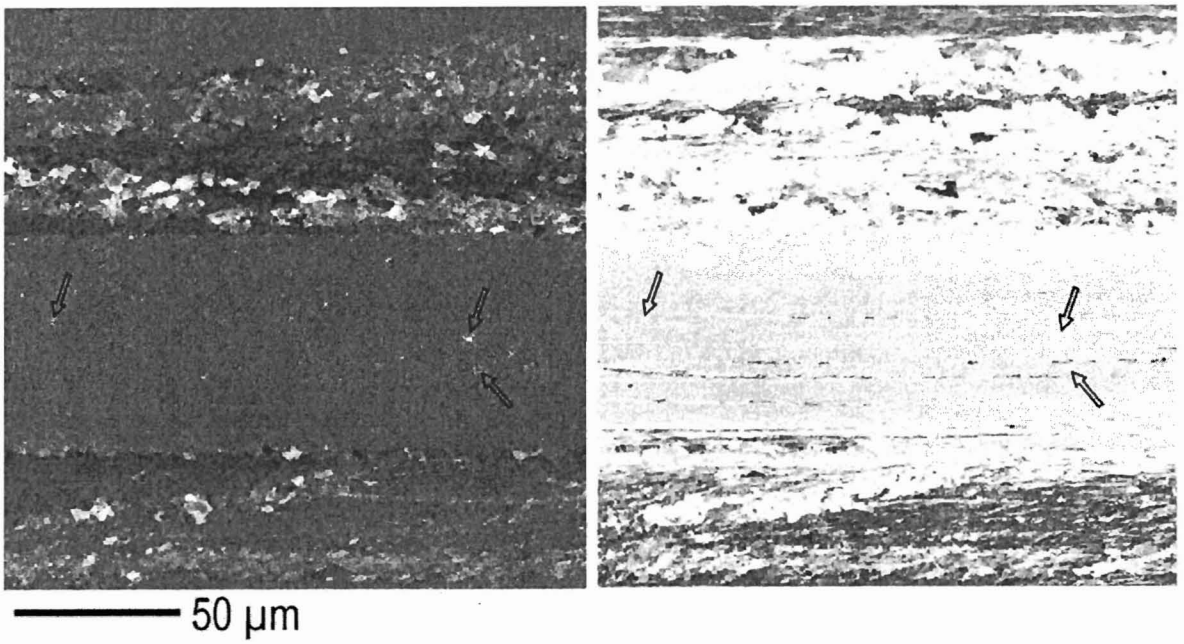

Figure 9. Rolling direction inverse-pole-figure map and rolling-texture-component map of as-rolled 5A3-1R. The arrows indicate highly-misoriented subgrains within the {110}<112> (copper) oriented band.

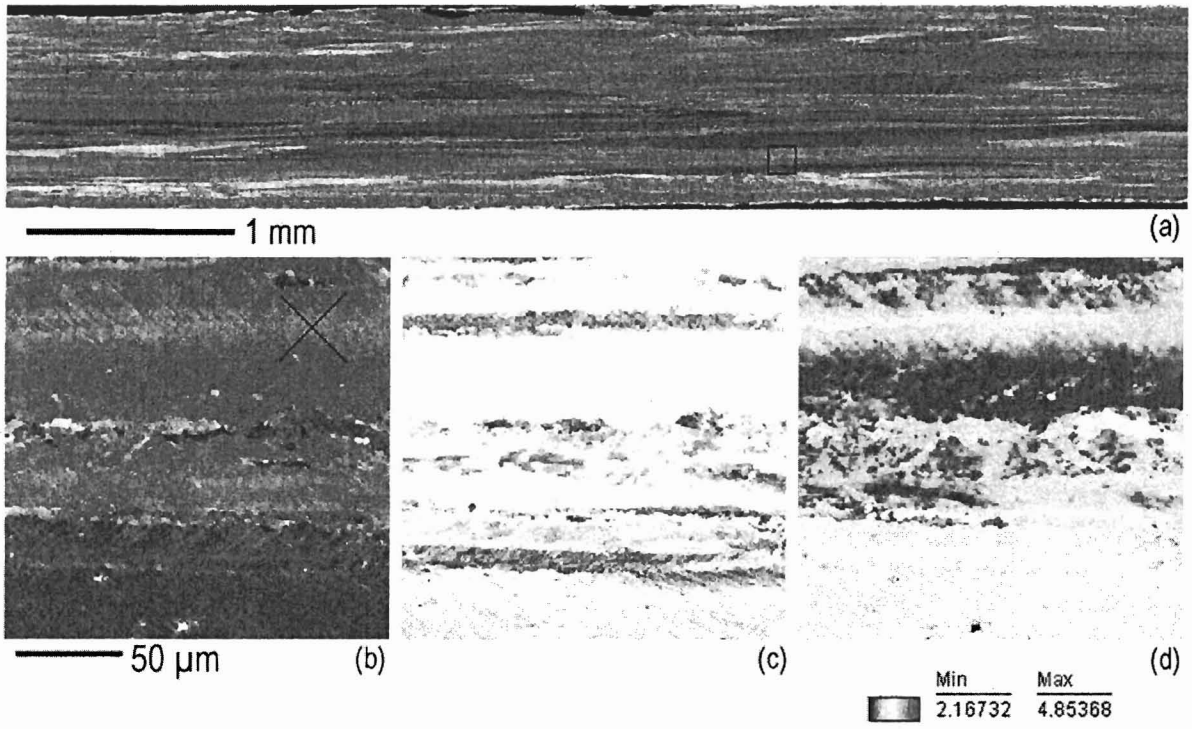

Figure 10. (a) Rolling-direction inverse-pole-figure-map, (b) higher resolution scan of the region enclosed by the black box in (a), (c) deformation-texture-component map, and (d) Taylor-factor map for sample 5A1-2R.

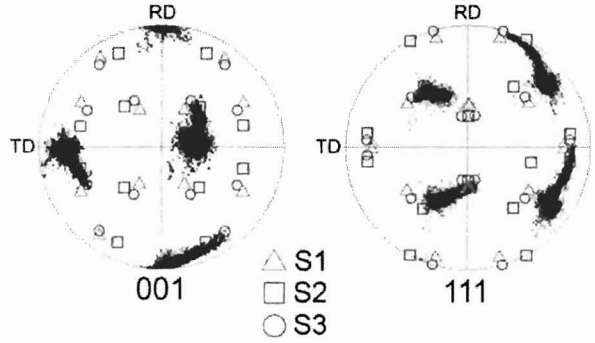

Figure 11. Discrete equal-angle pole figures showing the continuous nature of the evolution of a near-cube oriented band into the S3 orientation in sample 5A1-2R.

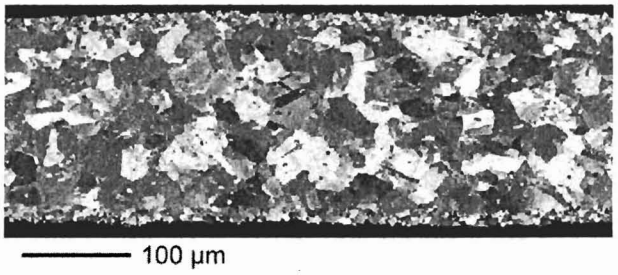

Figure 12. Rolling-direction inverse-pole-figure map of sample 5C8-3R.

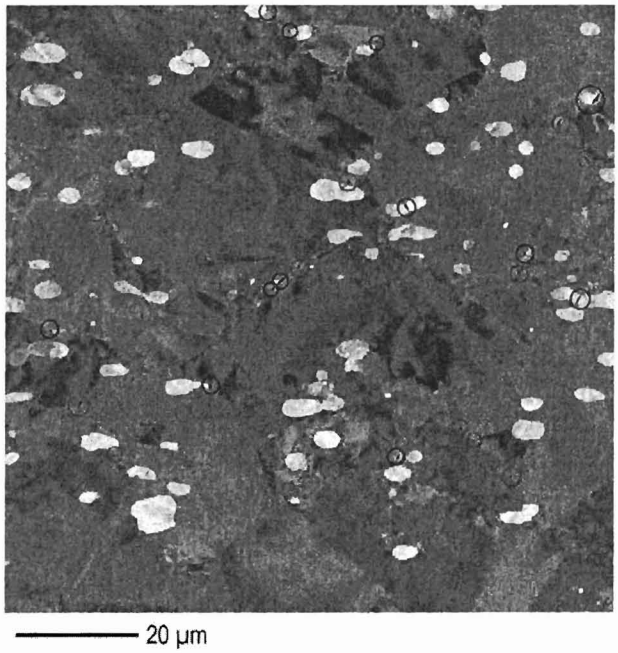

Figure 13. Backscattered electron image of rolled-and-flattened sample 5C8-3R. The red circles indicate voids at γ/γ grain boundaries; blue circles indicate voids at γ/γ' boundaries.

Figure 14. Rolling-direction inverse-pole-figure map of sample 5C9-1XR with image-quality overlay.

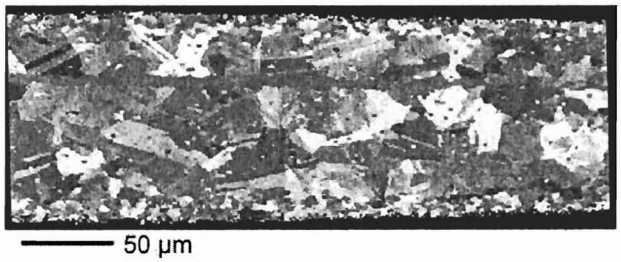

Figure 15. Rolling-direction inverse-pole-figure map of specimen 5C9-2XR.